



Published in final edited form as:

Cell Metab. 2014 December 2; 20(6): 1049–1058. doi:10.1016/j.cmet.2014.10.010.

Loss of White Adipose Hyperplastic Potential Is Associated with Enhanced Susceptibility to Insulin Resistance

Soo M. Kim¹, Mingyue Lun¹, Mei Wang², Samuel E. Senyo^{3,4,5}, Christelle Guillermier^{1,2,4}, Parth Patwari^{3,4}, and Matthew L. Steinhauser^{1,3,4,5,*}

¹Department of Medicine, Division of Genetics, Brigham and Women's Hospital, Boston, MA 02115, USA

²National Resource for Imaging Mass Spectroscopy, Brigham and Women's Hospital, Cambridge, MA 02138, USA

³Department of Medicine, Division of Cardiovascular Medicine, Brigham and Women's Hospital, Boston, MA 02115, USA

⁴Harvard Medical School, Boston, MA 02115, USA

⁵Harvard Stem Cell Institute, Cambridge, MA 02138, USA

SUMMARY

Fat mass expansion occurs by adipocyte hypertrophy or recruitment of differentiating adipocyte progenitors, the relative balance of which may impact systemic metabolism. We measured adipogenesis in murine subcutaneous (sWAT) and visceral white adipose tissue (vWAT) using stable isotope methodology and then modeled adipocyte turnover. Birth and death rates were similar within depots; however, turnover was higher in vWAT relative to sWAT. In juvenile mice, obesity increased adipogenesis, but in adults, this was only seen in vWAT after prolonged high-fat feeding. Statistical modeling suggests differentiation of adipocyte progenitors without an accompanying self-renewing division step may partially explain the age-dependent decline in hyperplastic potential. Additional metabolic interrogation of obese mice demonstrated an association between adipocyte turnover and insulin sensitivity. These data therefore identify adipocyte hypertrophy as the dominant mechanism of adult fat mass expansion and support the paradoxical concept that metabolic disease ensues due to a failure of adipose tissue plasticity.

*Correspondence: msteinhauser@partners.org.

SUPPLEMENTAL INFORMATION

Supplemental Information includes Supplemental Experimental Procedures, six figures, one table, and three data files and can be found with this article online at <http://dx.doi.org/10.1016/j.cmet.2014.10.010>.

AUTHOR CONTRIBUTIONS

S.M.K. performed animal experiments, tissue fractionation, and histology. M.L. performed histology and insulin measurements. M.W. and C.G. operated NanoSIMS instruments. S.E.S. assisted with mouse experiments and helped develop the IRMS approach. P.P. developed the modeling, wrote the code for all simulations, analyzed the modeling data, and assisted with writing the manuscript. M.L.S. designed the study, performed animal experiments, performed histology, performed IRMS measurements, analyzed the data, and wrote the manuscript. All authors approved the manuscript.

INTRODUCTION

The accepted paradigm of fat cell development holds that self-renewing adipocyte progenitors differentiate into mature lipid-storing adipocytes (Berry and Rodeheffer, 2013; Gupta et al., 2012; Rodeheffer et al., 2008; Tang et al., 2008). Although fat mass expansion may occur by generation of new fat cells (hyperplasia) or hypertrophy of existing adipocytes, the role of adipocyte hyperplasia at different developmental stages and with obesity is incompletely elucidated. Indeed, estimates of adult homeostatic adipogenesis vary by nearly two orders of magnitude (Jo et al., 2009; Neese et al., 2002; Rigamonti et al., 2011; Spalding et al., 2008; Wang et al., 2013). Moreover, while some studies suggest a role for adipocyte hyperplasia in the fat pad expansion seen with obesity (Ellis et al., 1990; Johnson et al., 1978; Lemonnier, 1972; Neese et al., 2002; Rigamonti et al., 2011), cytometric analyses (Hood and Allen, 1977; Salans et al., 1971, 1973) and recent ¹⁴carbon birth-dating experiments (Spalding et al., 2008) suggest that adipocyte number is fixed in adulthood.

Here, we adapted stable isotope methodology to measure adipogenesis, using thymidine, enriched to a high concentration (~97%) with the rare stable isotope of nitrogen (¹⁵N) as a tracer for cell division (Steinhauser et al., 2012). While conceptually similar to using radiolabeled thymidine or halogenated nucleotide analogs, stable isotopes provide several advantages (Steinhauser and Lechene, 2013; Stürup et al., 2008). First, stable isotopes are innocuous and therefore not associated with potential artifact from reagent toxicity. Second, observations made in model organisms can be tested with translational human studies due to the extensive precedent of safe human application. Third, mass spectrometry allows measurement of stable isotope tracers with high precision. In this study, we utilized isotope ratio mass spectrometry (IRMS) to measure tracer uptake in cell fractions isolated from adipose tissue and multi-isotope imaging mass spectrometry (MIMS) to quantitatively image stable isotopes in histologic sections. MIMS merges the precise tracer measurements with imaging resolution approaching transmission electron microscopy (Lechene et al., 2006; Steinhauser et al., 2012). We measured adipogenesis during aging and in obesity models, guided by the rationale that quantifying the dynamics of adipogenesis—and therefore testing for an association between adipogenesis and fat mass expansion—is a vital step in determining the role of adipocyte turnover in the pathophysiology of obesity.

RESULTS

Stable Isotope Methodology to Track Adipogenesis In Vivo

We measured incorporation of ¹⁵N-thymidine in replicating cells by an increase in ¹⁵N/¹⁴N above the natural ratio (0.37%), using two complementary mass spectrometry approaches (Figure 1A), MIMS and IRMS. Quantitative mass images rendered by MIMS reveal intracellular details, such as adipocyte nuclei, identifiable by their close association with a defining, large lipid droplet (Figure 1B and Figure S1 available online) and a shared plasma membrane. These features allow the discrimination of adipocytes from the less morphologically distinct and heterogenous interstitial cells, which include endothelial cells, fibroblasts, immune/inflammatory cells, and progenitors. For analyses described here,

adipocyte identity was determined based on these morphologic criteria from mass images by an observer unaware of experimental group and labeling data.

Stable isotope measurements are visually rendered by a hue saturation intensity (HSI) transformation (Figure 1C) (Lechene et al., 2006). The low end (blue) of the scale is set to natural abundance and the upper bound (red) set to emphasize regional differences in tracer incorporation; however, scale changes leave the underlying quantitative data unmodified. The rapidly dividing small intestine serves as a positive labeling control (Figure 1C). ^{15}N -labeling is concentrated specifically in the nucleus (Senyo et al., 2013; Steinhäuser et al., 2012). Labeling hotspots are observed throughout the nucleus, including condensed in close association to the nuclear membrane, a pattern expected of chromatin and comparable to that seen with DNA stains such as DAPI (Senyo et al., 2013). While we initially expected to see more cytoplasmic labeling due to mitochondrial DNA, this has not been evident even in mitochondrial rich tissues like the heart (Senyo et al., 2013), we speculate due to the extremely small size of the mitochondrial genome relative to nuclear DNA.

Although we previously detected rare cardiac myocyte division with MIMS, the analyses required ~1 year of instrument time (Senyo et al., 2013). WAT poses a similar challenge, due to the large size of adipocytes. A MIMS imaging plane (depth <1 nM) shows many adipocytes, however, adipocyte nuclei are infrequent. This provided rationale to use IRMS as a complementary, higher throughput approach. Analyses of WAT after pulse-chase administration of ^{15}N -thymidine to 4-week-old C57BL/6 mice, for example, showed increasing ^{15}N in adipocytes during chase, consistent with the differentiation of ^{15}N -labeled adipocyte progenitors; whereas, ^{15}N -signal in stromal-vascular cells from the same tissues showed a converse pattern of signal dilution, consistent with ongoing turnover (Figure 1D). In cell culture experiments, IRMS detected ^{15}N -thymidine labeling down to a frequency of ~1:500–1:1,000 cells (Figure S2). Therefore, this approach combines the sensitivity to detect infrequent cell divisions with higher throughput, making it ideally suited to measure relative differences in adipogenesis.

Adult vWAT Demonstrates Increased Adipogenesis Relative to sWAT

To establish basal adipocyte formation in adult WAT, we labeled 10-week-old C57BL/6 mice with ^{15}N -thymidine (20 $\mu\text{g}/\text{hr}$) for 8 weeks (Figure S3). Based on carbon birth-dating of human subcutaneous adipocytes, which showed an annual turnover rate of ~10% (Spalding et al., 2008), we predicted our analysis of 294 adipocyte nuclei would yield approximately five ^{15}N -labeled adipocytes. We detected 24 $^{15}\text{N}^+$ adipocyte nuclei (8.16%, pooled from $n = 3$ mice) (Figures 2A–2C); however, we also observed a marked interdepot difference. Whereas sWAT measurements were consistent with predictions from carbon birth dating (8 weeks: observed sWAT = 1.05%, expected = 1.54%, $\chi^2 p = 0.56$), we found a higher rate of adipogenesis in vWAT (21.57% versus 1.05%, $\chi^2 p < 0.0001$). $^{15}\text{N}^+$ adipocytes segregated into a distribution that was approximately normal (based on ^{15}N -intensity) and statistically distinct from the heterogeneous stromal vascular cells (Figure S4). Stromal-vascular cells were also labeled at a significantly higher frequency (sWAT SV = 32%, $n = 1,980$; vWAT SV = 63%, $n = 893$) compared to adipocytes from the same depot ($\chi^2 p < 0.0001$), consistent with a higher rate of stromal vascular cell turnover. $^{15}\text{N}^+$

adipocytes were also smaller than the unlabeled adipocytes (Figure 2C), consistent with the less mature state expected of recently differentiated adipocytes.

Cell division can also be measured during label-free chase by the predictable halving of label with each division (Steinhauser et al., 2012), an analysis made possible by quantitative sampling of nuclei (Figure S4). We therefore administered ^{15}N -thymidine to mice from postnatal day 4 through week 8 and analyzed WAT at two time points: at the end of the label and again after 18-month-long chase (Figure 3). Before chase, ^{15}N -labeling was detected in 56% and 85% of adipocytes in sWAT and vWAT, respectively (χ^2 , $p < 0.0001$). Unlabeled adipocytes at this time point likely arose from cells that were committed to an adipocyte fate prior to the onset of labeling at postnatal day 4. Therefore, the higher frequency of unlabeled adipocytes in sWAT (44%) compared to vWAT (15%) is consistent with the previously shown earlier developmental age of sWAT compared to vWAT (Wang et al., 2013).

After the 18 month chase, in addition to an interval increase in adipocyte size (Figures 3A and 3B), vWAT labeling was dramatically reduced. While the dilution of label was particularly marked in the heterogeneous stromal-vascular fraction (Figure 3C), there was also significant dilution of label in visceral adipocytes (Figure 3C), consistent with the moderate turnover rate predicted by our measurements of adipogenesis rate in adult mice (Figure 2).

Unexpectedly, subcutaneous adipocytes displayed an opposite pattern. Rather than dilution of label, we observed a significant and paradoxical increase in the ^{15}N -labeled cells after the 18 month chase (Figure 3C, χ^2 $p < 0.01$). Because ^{15}N -labeled adipocytes were smaller than the $^{15}\text{N}^-$ adipocytes (Figure 2C), one hypothesis for the label enrichment is that the rate of cell death is higher in the larger, and likely older, $^{15}\text{N}^-$ cells. The surviving cells would then be more likely to be $^{15}\text{N}^+$.

A second hypothesis for this pattern is that some adipocytes are formed from previously labeled adipocyte progenitors that then differentiated to generate new adipocytes without further division. In this case, the total adipocyte birth rate would be underestimated by pulse-labeling experiments. In addition, such a failure of progenitor self-renewal could lead to exhaustion of the pool, a phenomenon observed in genetic lineage tracing studies after prolonged administration of rosiglitazone, a PPAR γ agonist, which is thought to promote adipogenesis (Tang et al., 2011).

Adipocyte Birth without Accompanying Progenitor Cell Division Is Required to Explain ^{15}N -label Dynamics in sWAT

To test which of the proposed hypotheses correctly explain the paradoxical enrichment of $^{15}\text{N}^+$ cells in the sWAT during the 18 month chase, we developed a model to simulate adipocyte ^{15}N label status, birth, and death over this period. The model combined the information obtained from the adult label experiment with the observations made at the beginning of the chase to simulate the effects of changing multiple assumptions. This allowed us to test multiple hypotheses for the observed enrichment of ^{15}N -positive cells in the sWAT, as well as test the sensitivity of our conclusions to the assumptions made.

For the baseline model, we initially assumed birth and death rates were equal, based on previous work (Jo et al., 2010). To validate this assumption, we experimentally determined adipocyte number and volume in mice of varying ages and found no significant variation in number over the time period of the chase (Figure S6). However, simulation demonstrated that varying the assumed relationship between birth and death from zero cell death to as much as 50% increased cell death, the baseline model could not explain more than a 3% enrichment in $^{15}\text{N}^+$ cells in the sWAT (Figures 4A and 4B; Table S1). We furthermore considered the possibility that due to cell heterogeneity, the observed proportion of $^{15}\text{N}^+$ cells in the SV compartment underestimates the true proportion of $^{15}\text{N}^+$ preadipocytes. However, simulations showed that even assuming that all preadipocytes were $^{15}\text{N}^+$ over the entire chase, the turnover rate in the sWAT was not high enough to cause more than a 7% enrichment in $^{15}\text{N}^+$ adipocytes (“Pread. all $^{15}\text{N}^+$,” Figures 4A and 4B; Table S1).

Having rejected other hypotheses to explain the label enrichment, we incorporated into the model the increase in birth rate predicted in the case of adipocytes born without accompanying precursor cell division. Changing this assumption alone could explain an 8% enrichment in $^{15}\text{N}^+$ sWAT adipocytes (“ $f_{\text{DS}} = 1$ Model,” Figures 4A and 4B). Finally, combining differentiation without division and a preadipocyte $^{15}\text{N}^+$ underestimation rate that varied between sWAT and vWAT, produced a set of assumptions that was able to simulate the full 17% label enrichment in sWAT while maintaining label dilution in the vWAT (“Final Model,” Figures 4A and 4B; Table S1).

The final model of adipocyte turnover also predicts a depot difference in adipocyte death. We tested this prediction by a blinded histologic analysis of dead adipocytes, which are identifiable due to the characteristic influx of macrophages that surround the dead adipocyte, forming so-called “crown-like structures” (Murano et al., 2008) (Figure 4C). CLS were detected at higher frequencies in vWAT (Figure 4D), and the relative ratio between vWAT and sWAT CLS frequencies in the adult was consistent with adipocyte death as predicted by the model (Figure 4D; Table S1). Such empiric measurements of adipocyte death cannot be directly translated into a time-dependent death rate because the precise time to CLS clearance is unknown. However, these data are supportive of the “Final Model” in which adipocyte death is matched to adipocyte birth, the rate of which is due to progenitor differentiation, with and without preceding progenitor division.

Obesity-Related Adipocyte Hyperplasia Declines in the Adult

With limited sWAT plasticity during normal aging, what occurs with obesity? We first addressed this question in the diet-induced obesity model. C57BL/6 mice were randomly assigned to high-fat diet or control chow at 4 or 10 weeks of age, administered ^{15}N -thymidine pulse-chase, and followed by IRMS analysis of the adipocyte fractions. In 4-week-old mice, 5 weeks of high-fat feeding was associated with increased ^{15}N -labeling in both sWAT and vWAT adipocytes, consistent with increased adipogenesis (Figure 5A). A similar increase was not observed in adult mice, aged 10 weeks at study start. In a separate experiment, where a subset of 10-week-old mice were exposed to an 8 week run-in period of high-fat feeding, prior to 4 weeks of ^{15}N -thymidine labeling, a 57% increase ($p < 0.05$)

in ^{15}N -labeling was observed in adipocytes isolated from vWAT, but not from sWAT, suggesting some capacity for adipocyte hyperplasia in the visceral depot (Figure 5B).

We also tested for differences in proliferative activity in progenitor containing stromal vascular fractions. Mice received chow or high-fat diet for 8 weeks followed by ^{15}N -thymidine for 1 week. IRMS analysis of unsorted stromal vascular cells or those subjected to either negative selection (excluding lineage⁺ and CD31⁺ endothelial cells) or positive selection for PDGFR α -expressing cells (Berry and Rodeheffer, 2013), generally showed increased proliferative activity in vWAT compared to sWAT (Figure 5C). High-fat feeding had a modest effect on ^{15}N -labeling in sWAT, only reaching statistical significance in the unsorted population. However, a robust increase in ^{15}N -signal was detected the PDGFR α ⁺ fraction of vWAT after high-fat feeding. Because the stromal vascular cell fraction is comprised of a heterogeneous array of cell types, including endothelial cells, fibroblasts, macrophages, and progenitors, these analyses must be interpreted with caution, but taken together the results are largely consistent with concept that vWAT has a higher turnover rate than sWAT.

We also performed an evaluation of adipogenesis in a more extreme model of obesity, the *Lepr^{db}/Lepr^{db}* (db/db) mouse. Mice received a 2 week pulse of ^{15}N -thymidine followed by a 4 week label-free chase. Compared to WT mice on the same background, 4-week-old db/db mice demonstrated significant increases in adipocyte labeling in both sWAT and vWAT, although this effect was lost in adult mice (Figure 5D). If the db/db mice emerged from postnatal development with more adipocytes, as predicted by the higher level of labeling in the young mice, then the same relative rate of turnover (and therefore relative level of ^{15}N -labeling) would equal a higher absolute rate of adipogenesis. This observation is also consistent with predictions from a model of human adipocyte turnover, where obesity that was initiated prior to adulthood resulted in a higher number of adipocytes, a higher absolute rate of new adipocyte formation, but similar rates of relative turnover (Spalding et al., 2008).

Given the process entailed in isolating and purifying adipocytes from the heterogeneous stromal vascular cells, it is important to consider possible sources of bias arising from an impure adipocyte preparation or the preferential loss of large adipocytes. Larger adipocytes are presumably older and unlabeled and therefore their selective loss during isolation would result in a falsely elevated $^{15}\text{N}/^{14}\text{N}$ ratio. Because obesity leads to increased proliferation of stromal-vascular elements, including infiltrating inflammatory cells, the contamination of the adipocyte fraction by proliferative stromal vascular cells would also cause a falsely elevated $^{15}\text{N}/^{14}\text{N}$ ratio. Therefore, both scenarios should lead to a false positive association between fat pad expansion and adipogenesis, not the flat response observed in the adult. Nonetheless, due to these potential sources of bias and given the observed interanimal variance in ^{15}N -labeling, we cannot exclude small differences in adipocyte turnover in the adult obesity models. However, taken together with the association between obesigenic stimuli and increased adipocyte size (Figures 5E and 5F), we conclude that adipocyte hypertrophy is the dominant mechanism of fat mass expansion in adult obesity.

sWAT Adipocyte Turnover Predicts Insulin Sensitivity with Obesity

A number of studies in animal models and humans have found adipocyte hypertrophy to predict metabolic disease (Kabir et al., 2011; Weyer et al., 2000), whereas a cross-sectional human study suggests that a hyperplastic tendency is predictive of metabolic health (Arner et al., 2010). In the absence of a strong association between adipocyte birth and fat mass expansion in the adult, we hypothesized that adipocyte turnover is metabolically beneficial. To test this, we applied quantitative stable isotope methodology to measure adipogenesis in two obesigenic mouse strains previously found to have different metabolic profiles, the C57BL/6 and AKR mice (Rossmeisl et al., 2003).

Adult male mice of both strains ($n = 8$) were started on a high-fat diet at 8 weeks of age. Mice underwent ^{15}N -thymidine labeling starting 4 weeks into high-fat feeding and metabolic parameters were assessed after a total of 8 weeks on the high-fat diet. Both strains gained a significant and similar amount of weight (Figure 6A). Although the C57BL/6 mice had higher serum glucose levels after an overnight fast (C57BL/6 = 75.6 ± 3.1 mg/dl, AKR = 59.4 ± 4.7 mg/dl, $p < 0.05$), the response to a 1 g/kg intraperitoneal glucose tolerance test was similar between the two strains (Figure 6B). In contrast, the AKR mice demonstrated more severe insulin resistance, both on the basis of a blunted response to an intraperitoneal insulin tolerance test (0.75 U/kg) and significantly higher serum insulin levels at the time of sacrifice (Figures 6C and 6D).

Although both strains showed a similar pattern of weight gain on a high-fat diet, there was a trend toward larger adipocytes in AKR mice (Figure 6E, sWAT $p = 0.1$, vWAT $p = 0.1$). Conversely, an IRMS analysis demonstrated significantly higher ^{15}N -labeling of both visceral and subcutaneous adipocytes from C57BL/6 mice compared to AKR mice, consistent with an increased rate of adipogenesis (Figure 6F) and a linear regression analysis showed an inverse association between sWAT adipogenesis (^{15}N labeling) and serum insulin levels (Figure 6G). Together, these data support the concept that a failure of adipose tissue plasticity is associated with insulin resistance.

DISCUSSION

The adipocyte is increasingly recognized as a regulator of energy balance, systemic metabolism, and inflammation (Cristancho and Lazar, 2011). Despite the intuitive appeal of targeting adipocytes as a pathologic component of obesity, a number of often-cited observations support the concept that a dynamic adipocyte pool may be beneficial in states of excess energy consumption. Stimulation of PPAR γ -dependent adipogenesis with thiazolidinedione drugs, for example, is associated with an insulin sensitizing effect, although distinguishing the specific effects of PPAR γ activation responsible for this beneficial property is an area of active research (Choi et al., 2010). Conversely, impaired adipocyte development is associated with insulin resistance in a number of circumstances. For example, both mice and humans with lipodystrophy demonstrate severe insulin resistance (Moitra et al., 1998; Pajvani et al., 2005; Seip, 1959). Therefore, an open question is whether adipogenesis is an adaptive or maladaptive response in obesity.

Here, we developed a stable isotope approach to track adipogenesis, guided by the rationale that testing for associations between adipogenesis and obesity will lend insight into the contribution of fat cell development to disease pathogenesis. We show a marked age-dependent decline in homeostatic and obesity-related adipocyte plasticity. These data largely converge with older studies (Greenwood and Hirsch, 1974; Salans et al., 1971) and more recent ^{14}C birth dating (Spalding et al., 2008) in showing limited capacity for dynamic changes in adipocyte number in adults. We speculate that studies reporting substantially higher rates of adipocyte birth may reflect the challenge of distinguishing slowly dividing cell populations, such as adipocytes, from surrounding stromal-vascular cells that divide at higher rates (Klyde and Hirsch, 1979). We propose that this study is less prone to such bias due to the superior imaging resolution of MIMS and the quantitative precision of stable isotope methodology.

Our data point to a mechanism for limited plasticity of adipose tissue, the phenomenon of progenitor differentiation without preceding division (Figures 3 and 4). Without the stem cell property of self-renewal—or the clonal expansion step that precedes terminal differentiation in preadipocyte cell lines—the adipocyte progenitor pool may be programmed for exhaustion. If future studies confirm this phenomenon, it could represent an important mechanism of adipose tissue aging and functional decline with obesity. Moreover, with an inverse association between sWAT adipocyte turnover and insulin resistance, the intrinsic capacity for progenitor self-renewal represents an additional link between local adipose tissue function and systemic metabolism (Cohen et al., 2014; Tran et al., 2008).

An important question raised by these data then is whether there are any contexts in which adult WAT becomes hyperplastic. Indeed, this study does not exclude the possibility that adipogenesis is dynamically regulated in contexts outside of the standard obesity models used here, which were conducted with male mice. Given apparent gender differences in adiposity and propensity for adipocyte hypertrophy (Drolet et al., 2008; Lemieux et al., 1993), for example, sex may represent an important determinant of adipocyte progenitor function and WAT hyperplastic potential. In addition, the close association of adipocyte birth and death (Figure 4), also predicted from human modeling (Spalding et al., 2008), raises the possibility that an increase in adipocyte death would result in increased adipocyte birth. Interestingly, the one condition in the adult where we observed a modest, yet statistically significant, increase in adipogenesis was in the visceral depot after prolonged high-fat feeding (Figure 5), a condition also known to be associated with increased adipocyte death (Alkhoury et al., 2010). Moreover, a robust example of induced de novo adipocyte birth in the adult mouse occurs in response to widespread, programmed adipocyte apoptosis (Pajvani et al., 2005); therefore we speculate that adipocyte death is a causal determinant of adipogenesis.

From a methodological standpoint, it is important that our results demonstrate limited WAT plasticity, similar to studies using genetic lineage tracing (Wang et al., 2013) or ^{14}C -birthdating (Spalding et al., 2008). The relative agreement of these approaches suggests that they can be considered complementary tools to study adipocyte turnover. We anticipate that this study will provide a valuable template for future in vivo studies of adipogenesis, in large part due to the flexibility conferred by stable isotope tracers and their easy applicability to a

wide-range of experimental models, including genetic models displaying obesity or metabolic phenotypes. Perhaps most important is the possibility of conducting prospective studies in humans, due to the extensive precedent of safe application of stable isotope methodology in human studies (Steinhauser and Lechene, 2013).

This study demonstrates that lack of adipogenesis, as opposed to adipogenesis, may be the maladaptive contributor to obesity-related diabetes mellitus. This is consistent with the intriguing hypothesis that diabetes mellitus arises from a failure of WAT plasticity (Heilbronn et al., 2004; McLaughlin et al., 2007; Pasarica et al., 2009; Wang et al., 2013). Therefore, this study provides additional rationale to test whether limitations in WAT progenitor self-renewal and differentiation are causally linked to obesity-related diseases.

EXPERIMENTAL PROCEDURES

Mouse Studies

Experiments were approved by the Harvard Medical Area Standing Committee on Animals. Male C57Bl/6 mice were purchased from Charles River. Male *Lepr^{db}/Lepr^{db}* mice and male WTs of the same background (C57BLKS/J) were purchased from Jackson Laboratories. Male AKR mice were purchased from Jackson Laboratories. Mice were housed at 22°C ± 2°C, with a 12 hr light (0700–1900 hr), 12 hr dark (1900–0700 hr) cycle and free access to food and water. Aging studies and those using *Lepr^{db}/Lepr^{db}* mice were conducted with a diet containing 23% protein, 21% fat, and 55% carbohydrates (PicoLab Mouse Diet 20). Diet-induced obesity was modeled with high fat (D12492) and control chow (D12450J) matched for sucrose content (Research Diets). Insulin tolerance tests were performed by injecting 0.75 U/kg regular insulin intraperitoneally (i.p.) after 4 hr of fasting. Glucose tolerance tests were performed by i.p. injection of glucose (1 g/kg) after an overnight fast. Blood was collected from the tail vein and measured by glucometer (Contour, Bayer). Serum was collected at the time of sacrifice and insulin measured by ELISA (Millipore).

Stable Isotopes

¹⁵N-thymidine (Cambridge Isotope Laboratories) was dissolved in water (20 mg/ml). Prior to 4 weeks, mice were administered 50 µg/g/dose by subcutaneous injection (Hamilton syringe, 31 g needle) every 12 hr. For long-term labeling studies, mice 4 weeks or older were implanted with subcutaneous osmotic minipumps (Alzet), delivering 20 µg/hr continuously. For shorter term labeling studies in DIO or db/db mice, ¹⁵N-thymidine was administered by subcutaneous injection (25 µg/g) every 12 hr.

MIMS

MIMS was performed as previously described (Steinhauser et al., 2012) using the prototype instrument and the NanoSIMS 50L (Cameca). Tissue was fixed (4% paraformaldehyde), embedded in LR white, sectioned (0.5 µm), and mounted on silicon chips. Samples were analyzed in automated chain analysis mode, with each tile acquired at 256 × 256 pixels, 60 µm × 60 µm field size. Nuclei were manually traced in a customized plugin to ImageJ (OpenMIMS: <http://nrims.harvard.edu/software>) and assigned an identity of adipocyte, stromal-vascular cell, or possible adipocyte by an observer unaware of fat depot,

experimental group, or labeling status of the cell. Typical reasons for the designation of “possible adipocyte” included imaging artifact (e.g., nucleus found at the margin of two adjacent fields) or inability to clearly distinguish a close association with a lipid droplet and shared plasma membrane. In these cases, the specific cell was reimaged at higher resolution (512×512 pixels, 10–25 μm raster size) and the images reevaluated by a blinded observer. Cross-sectional area was calculated by tracing the adipocyte periphery in ImageJ.

IRMS

Adipose tissue was minced and digested with collagenase type D (Roche) in a shaking water bath (37°C, 225 rpm, 40 min). The digest was filtered (300 μm nylon mesh, Spectrum Labs) and centrifuged at $400 \times g$ for 10 min. Adipocytes were collected and washed two times with PBS. Pelleted stromal vascular cells were strained (40 μm) and then washed with PBS. For analyses of stromal-vascular subfractions, cells were subjected to additional positive (PDGFR α +) or negative selection (lineage $^{-}$) using antibody-coated microbeads (Miltenyi Biotec). Cells were aliquoted into tin cups and dried at 60°C. For analyses of genomic DNA, cells were directly lysed in DNazole (MRC). Because of the possibility of finding small (<300 μm) incompletely digested tissue fragments containing stromal vascular cells adherent to buoyant adipocytes floating in the supernatant, analysis of aliquots of DAPI-stained adipocytes served as a quality control metric. This analysis reproducibly yielded an adipocyte preparation with minimal contamination from adherent nonadipocytes ($\approx 98\%$). Samples were introduced to an elemental analyzer (Vario Pyrocube, Elementar) coupled to an IRMS (Isoprime 100, Elementar). Tuning was confirmed with urea standards. Samples obtained from unlabeled mice were used as the natural background. Data were expressed as % above natural ratio, a value obtained by the following equation: $100 \times (\text{Sample} - \text{Control})/0.37$.

Histology

Adipose tissue specimens were fixed with 4% paraformaldehyde, paraffin-embedded, sectioned, and stained using standard methods. Cross-sectional areas of adipocytes in hematoxylin and eosin (H&E)-stained sections were calculated by tracing the adipocyte periphery in ImageJ by a blinded observer. For immunohistochemistry, an antigen retrieval step was used by heating samples in a citrate-based buffer (Dako) at 95°C for 20 min. A rat monoclonal primary antibody to murine F4/80 (Abcam) was used at a concentration of 1:250 for 1 hr at room temperature. Endogenous peroxidase activity was quenched with a 20 min incubation in 0.3% H_2O_2 . A mouse adsorbed and biotinylated goat anti-rat IgG secondary antibody was used at a concentration of 1:250 for 1 hr, followed by ABC reagent and DAB (Vector Laboratories). “Crown like structures” were identified and counted by an observer, blinded to depot and experimental group.

Statistics

Statistical analyses were performed with Jmp10.0 and Prism 6.0. The Student’s t test was used to compare two, independent, normally distributed groups and the Mann-Whitney test used when one or more groups did not pass a Shapiro-Wilk normality test. The Kruskal-Wallis test was used to compare non-normally distributed data involving multiple groups,

with significance assigned for $\alpha < 0.05$ after a Dunn's multiple comparison correction. Proportions were compared using the χ^2 test. A p value < 0.05 on a two-tailed test was used to indicate significance.

Supplementary Material

Refer to Web version on PubMed Central for supplementary material.

Acknowledgments

We thank C. Lechene for critical feedback and the National Resource for Imaging Mass Spectrometry where NanoSIMS analyses were conducted. We thank R. Lee for critical feedback. We thank P. Cohen, J. Brown, and W. Chutkow for critical evaluation of the manuscript. S.E.S is funded by the NIH (HL108570). M.L.S. is funded by the Harvard Stem Cell Institute, the Brigham and Women's Hospital Watkins Cardiovascular Leadership Award, and the NIH (DK090147).

References

- Alkhoury N, Gornicka A, Berk MP, Thapaliya S, Dixon LJ, Kashyap S, Schauer PR, Feldstein AE. Adipocyte apoptosis, a link between obesity, insulin resistance, and hepatic steatosis. *J Biol Chem*. 2010; 285:3428–3438. [PubMed: 19940134]
- Arner E, Westermark PO, Spalding KL, Britton T, Rydén M, Frisén J, Bernard S, Arner P. Adipocyte turnover: relevance to human adipose tissue morphology. *Diabetes*. 2010; 59:105–109. [PubMed: 19846802]
- Berry R, Rodeheffer MS. Characterization of the adipocyte cellular lineage in vivo. *Nat Cell Biol*. 2013; 15:302–308. [PubMed: 23434825]
- Choi JH, Banks AS, Estall JL, Kajimura S, Boström P, Laznik D, Ruas JL, Chalmers MJ, Kamenecka TM, Blüher M, et al. Anti-diabetic drugs inhibit obesity-linked phosphorylation of PPARgamma by Cdk5. *Nature*. 2010; 466:451–456. [PubMed: 20651683]
- Cohen P, Levy JD, Zhang Y, Frontini A, Kolodin DP, Svensson KJ, Lo JC, Zeng X, Ye L, Khandekar MJ, et al. Ablation of PRDM16 and beige adipose causes metabolic dysfunction and a subcutaneous to visceral fat switch. *Cell*. 2014; 156:304–316. [PubMed: 24439384]
- Cristancho AG, Lazar MA. Forming functional fat: a growing understanding of adipocyte differentiation. *Nat Rev Mol Cell Biol*. 2011; 12:722–734. [PubMed: 21952300]
- Drolet R, Richard C, Sniderman AD, Mailloux J, Fortier M, Huot C, Rhéaume C, Tchernof A. Hypertrophy and hyperplasia of abdominal adipose tissues in women. *Int J Obes (Lond)*. 2008; 32:283–291. [PubMed: 17726433]
- Ellis JR, McDonald RB, Stern JS. A diet high in fat stimulates adipocyte proliferation in older (22 month) rats. *Exp Gerontol*. 1990; 25:141–148. [PubMed: 2369929]
- Greenwood MR, Hirsch J. Postnatal development of adipocyte cellularity in the normal rat. *J Lipid Res*. 1974; 15:474–483. [PubMed: 4415153]
- Gupta RK, Mepani RJ, Kleiner S, Lo JC, Khandekar MJ, Cohen P, Frontini A, Bhowmick DC, Ye L, Cinti S, Spiegelman BM. Zfp423 expression identifies committed preadipocytes and localizes to adipose endothelial and perivascular cells. *Cell Metab*. 2012; 15:230–239. [PubMed: 22326224]
- Heilbronn L, Smith SR, Ravussin E. Failure of fat cell proliferation, mitochondrial function and fat oxidation results in ectopic fat storage, insulin resistance and type II diabetes mellitus. *Int J Obes Relat Metab Disord*. 2004; 28(Suppl 4):S12–S21. [PubMed: 15592481]
- Hood RL, Allen CE. Cellularity of porcine adipose tissue: effects of growth and adiposity. *J Lipid Res*. 1977; 18:275–284. [PubMed: 864321]
- Jo J, Gavrilova O, Pack S, Jou W, Mullen S, Sumner AE, Cushman SW, Perival V. Hypertrophy and/or Hyperplasia: Dynamics of Adipose Tissue Growth. *PLoS Comput Biol*. 2009; 5:e1000324. [PubMed: 19325873]

- Jo J, Guo J, Liu T, Mullen S, Hall KD, Cushman SW, Periwé V. Hypertrophy-driven adipocyte death overwhelms recruitment under prolonged weight gain. *Biophys J*. 2010; 99:3535–3544. [PubMed: 21112277]
- Johnson PR, Stern JS, Greenwood MR, Hirsch J. Adipose tissue hyperplasia and hyperinsulinemia on Zucker obese female rats: a developmental study. *Metabolism*. 1978; 27(12, Suppl 2):1941–1954. [PubMed: 723643]
- Kabir M, Stefanovski D, Hsu IR, Iyer M, Woolcott OO, Zheng D, Catalano KJ, Chiu JD, Kim SP, Harrison LN, et al. Large size cells in the visceral adipose depot predict insulin resistance in the canine model. *Obesity (Silver Spring)*. 2011; 19:2121–2129. [PubMed: 21836643]
- Klyde BJ, Hirsch J. Isotopic labeling of DNA in rat adipose tissue: evidence for proliferating cells associated with mature adipocytes. *J Lipid Res*. 1979; 20:691–704. [PubMed: 490048]
- Lechene C, Hillion F, McMahon G, Benson D, Kleinfeld AM, Kampf JP, Distel D, Luyten Y, Bonventre J, Hentschel D, et al. High-resolution quantitative imaging of mammalian and bacterial cells using stable isotope mass spectrometry. *J Biol*. 2006; 5:20. [PubMed: 17010211]
- Lemieux S, Prud'homme D, Bouchard C, Tremblay A, Després JP. Sex differences in the relation of visceral adipose tissue accumulation to total body fatness. *Am J Clin Nutr*. 1993; 58:463–467. [PubMed: 8379501]
- Lemonnier D. Effect of age, sex, and sites on the cellularity of the adipose tissue in mice and rats rendered obese by a high-fat diet. *J Clin Invest*. 1972; 51:2907–2915. [PubMed: 5080416]
- McLaughlin T, Sherman A, Tsao P, Gonzalez O, Yee G, Lamendola C, Reaven GM, Cushman SW. Enhanced proportion of small adipose cells in insulin-resistant vs insulin-sensitive obese individuals implicates impaired adipogenesis. *Diabetologia*. 2007; 50:1707–1715. [PubMed: 17549449]
- Moitra J, Mason MM, Olive M, Krylov D, Gavriloova O, Marcus-Samuels B, Feigenbaum L, Lee E, Aoyama T, Eckhaus M, et al. Life without white fat: a transgenic mouse. *Genes Dev*. 1998; 12:3168–3181. [PubMed: 9784492]
- Murano I, Barbatelli G, Parisani V, Latini C, Muzzonigro G, Castellucci M, Cinti S. Dead adipocytes, detected as crown-like structures, are prevalent in visceral fat depots of genetically obese mice. *J Lipid Res*. 2008; 49:1562–1568. [PubMed: 18390487]
- Neese RA, Misell LM, Turner S, Chu A, Kim J, Cesar D, Hoh R, Antelo F, Strawford A, McCune JM, et al. Measurement in vivo of proliferation rates of slow turnover cells by 2H2O labeling of the deoxyribose moiety of DNA. *Proc Natl Acad Sci USA*. 2002; 99:15345–15350. [PubMed: 12424339]
- Pajvani UB, Trujillo ME, Combs TP, Iyengar P, Jelicks L, Roth KA, Kitsis RN, Scherer PE. Fat apoptosis through targeted activation of caspase 8: a new mouse model of inducible and reversible lipodystrophy. *Nat Med*. 2005; 11:797–803. [PubMed: 15965483]
- Pasarica M, Xie H, Hymel D, Bray G, Greenway F, Ravussin E, Smith SR. Lower total adipocyte number but no evidence for small adipocyte depletion in patients with type 2 diabetes. *Diabetes Care*. 2009; 32:900–902. [PubMed: 19228873]
- Rigamonti A, Brennand K, Lau F, Cowan CA. Rapid cellular turnover in adipose tissue. *PLoS ONE*. 2011; 6:e17637. [PubMed: 21407813]
- Rodeheffer MS, Birsoy K, Friedman JM. Identification of white adipocyte progenitor cells in vivo. *Cell*. 2008; 135:240–249. [PubMed: 18835024]
- Rossmeisl M, Rim JS, Koza RA, Kozak LP. Variation in type 2 diabetes—related traits in mouse strains susceptible to diet-induced obesity. *Diabetes*. 2003; 52:1958–1966. [PubMed: 12882911]
- Salans LB, Horton ES, Sims EA. Experimental obesity in man: cellular character of the adipose tissue. *J Clin Invest*. 1971; 50:1005–1011. [PubMed: 5552403]
- Salans LB, Cushman SW, Weismann RE. Studies of human adipose tissue. Adipose cell size and number in nonobese and obese patients. *J Clin Invest*. 1973; 52:929–941. [PubMed: 4693656]
- Seip M. Lipodystrophy and gigantism with associated endocrine manifestations. A new diencephalic syndrome? *Acta Paediatr*. 1959; 48:555–574. [PubMed: 14444642]
- Senyo SE, Steinhauser ML, Pizzimenti CL, Yang VK, Cai L, Wang M, Wu TD, Guerin-Kern JL, Lechene CP, Lee RT. Mammalian heart renewal by pre-existing cardiomyocytes. *Nature*. 2013; 493:433–436. [PubMed: 2322518]

- Spalding KL, Arner E, Westermark PO, Bernard S, Buchholz BA, Bergmann O, Blomqvist L, Hoffstedt J, Näslund E, Britton T, et al. Dynamics of fat cell turnover in humans. *Nature*. 2008; 453:783–787. [PubMed: 18454136]
- Steinhauser ML, Lechene CP. Quantitative imaging of subcellular metabolism with stable isotopes and multi-isotope imaging mass spectrometry. *Semin Cell Dev Biol*. 2013; 24:661–667. [PubMed: 23660233]
- Steinhauser ML, Bailey AP, Senyo SE, Guillemier C, Perlstein TS, Gould AP, Lee RT, Lechene CP. Multi-isotope imaging mass spectrometry quantifies stem cell division and metabolism. *Nature*. 2012; 481:516–519. [PubMed: 22246326]
- Stürup S, Hansen HR, Gammelgaard B. Application of enriched stable isotopes as tracers in biological systems: a critical review. *Anal Bioanal Chem*. 2008; 390:541–554. [PubMed: 17917720]
- Tang W, Zeve D, Suh JM, Bosnakovski D, Kyba M, Hammer RE, Tallquist MD, Graff JM. White fat progenitor cells reside in the adipose vasculature. *Science*. 2008; 322:583–586. [PubMed: 18801968]
- Tang W, Zeve D, Seo J, Jo AY, Graff JM. Thiazolidinediones regulate adipose lineage dynamics. *Cell Metab*. 2011; 14:116–122. [PubMed: 21723509]
- Tran TT, Yamamoto Y, Gesta S, Kahn CR. Beneficial effects of subcutaneous fat transplantation on metabolism. *Cell Metab*. 2008; 7:410–420. [PubMed: 18460332]
- Wang QA, Tao C, Gupta RK, Scherer PE. Tracking adipogenesis during white adipose tissue development, expansion and regeneration. *Nat Med*. 2013; 19:1338–1344. [PubMed: 23995282]
- Weyer C, Foley JE, Bogardus C, Tataranni PA, Pratley RE. Enlarged subcutaneous abdominal adipocyte size, but not obesity itself, predicts type II diabetes independent of insulin resistance. *Diabetologia*. 2000; 43:1498–1506. [PubMed: 11151758]

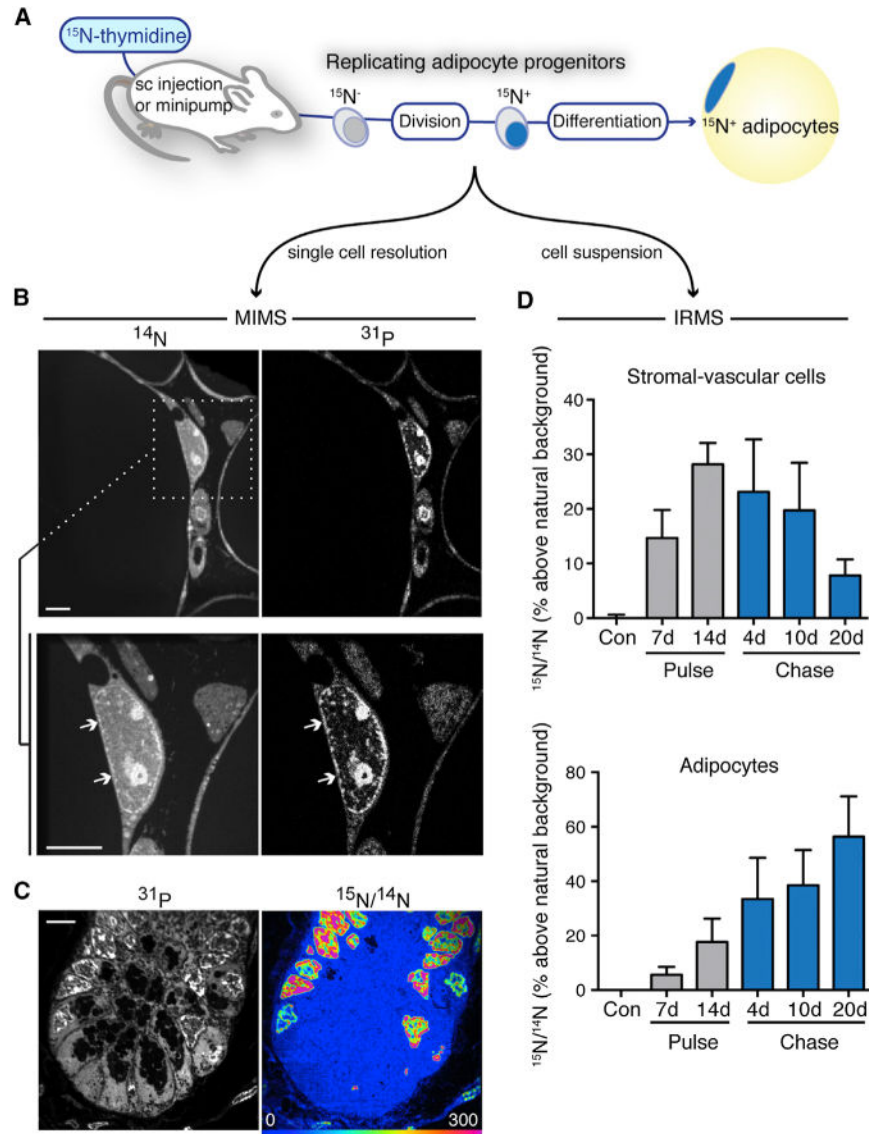


Figure 1. Tracking Adipogenesis in White Adipose Tissue with Stable Isotopes

(A) ^{15}N -thymidine labels dividing cells. (MIMS) measures label at the single cell level. Isotope ratio mass spectrometry (IRMS) is used for bulk analyses (e.g., a suspension of cells isolated from an individual depot).

(B) ^{14}N images show white tissue adipose (WAT) architecture and subcellular details, such as nuclei (white arrows). High phosphorus content in membranes and chromatin accounts for signal in ^{31}P images. Regions of interest (white box) can be reanalyzed at higher resolution. An adipocyte nucleus (white arrows) is seen adjacent to the lipid droplet, which has low nitrogen counts, and therefore appears dark. Scale bar represents 5 μm .

(C) Small intestinal crypt (+ control) after ^{15}N -thymidine. HSI $^{15}\text{N}/^{14}\text{N}$ image shows label localized to P-rich regions in the nucleus in a pattern resembling chromatin. The scale is set so blue is at natural abundance; blue regions (e.g., cytoplasm) are unlabeled. Scale bar represents 5 μm .

(D) Analysis of sWAT adipogenesis by ^{15}N -thymidine pulse-chase in 4-week-old mice (mean \pm SEM; n = 3–4 mice per time point). Label taken up in the heterogeneous stromal vascular cell fraction (top) during pulse faded with chase, consistent with cell turnover. Adipocyte labeling trended upward ($p < 0.05$) during chase, consistent with differentiation of labeled progenitors into adipocytes. See also Figures S1 and S2.

Author Manuscript

Author Manuscript

Author Manuscript

Author Manuscript

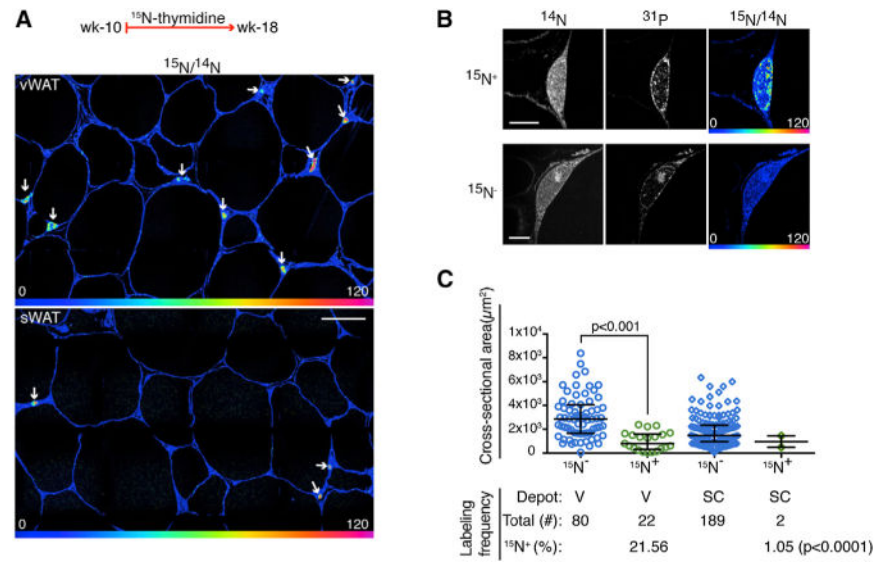


Figure 2. Depot-Specific Differences in Adult Adipogenesis

(A) ^{15}N -thymidine administered from postnatal weeks 10–18. Higher frequency of ^{15}N -nuclear labeling (white arrows) in vWAT (top) compared to sWAT (bottom). HSI mosaic images constructed from 60 μm tiles, scale bar represents 30 μm .

(B) Top: ^{15}N -labeled adipocyte. Bottom: ^{15}N -unlabeled adipocyte. Scale bar represents 5 μm .

(C) New ($^{15}\text{N}^+$) adipocytes are smaller than older ($^{15}\text{N}^-$) adipocytes as shown by area distribution. Bottom shows corresponding adipocyte labeling frequencies in the two depots. Pooled analysis of $n = 3$ mice.

See also Figures S3 and S4.

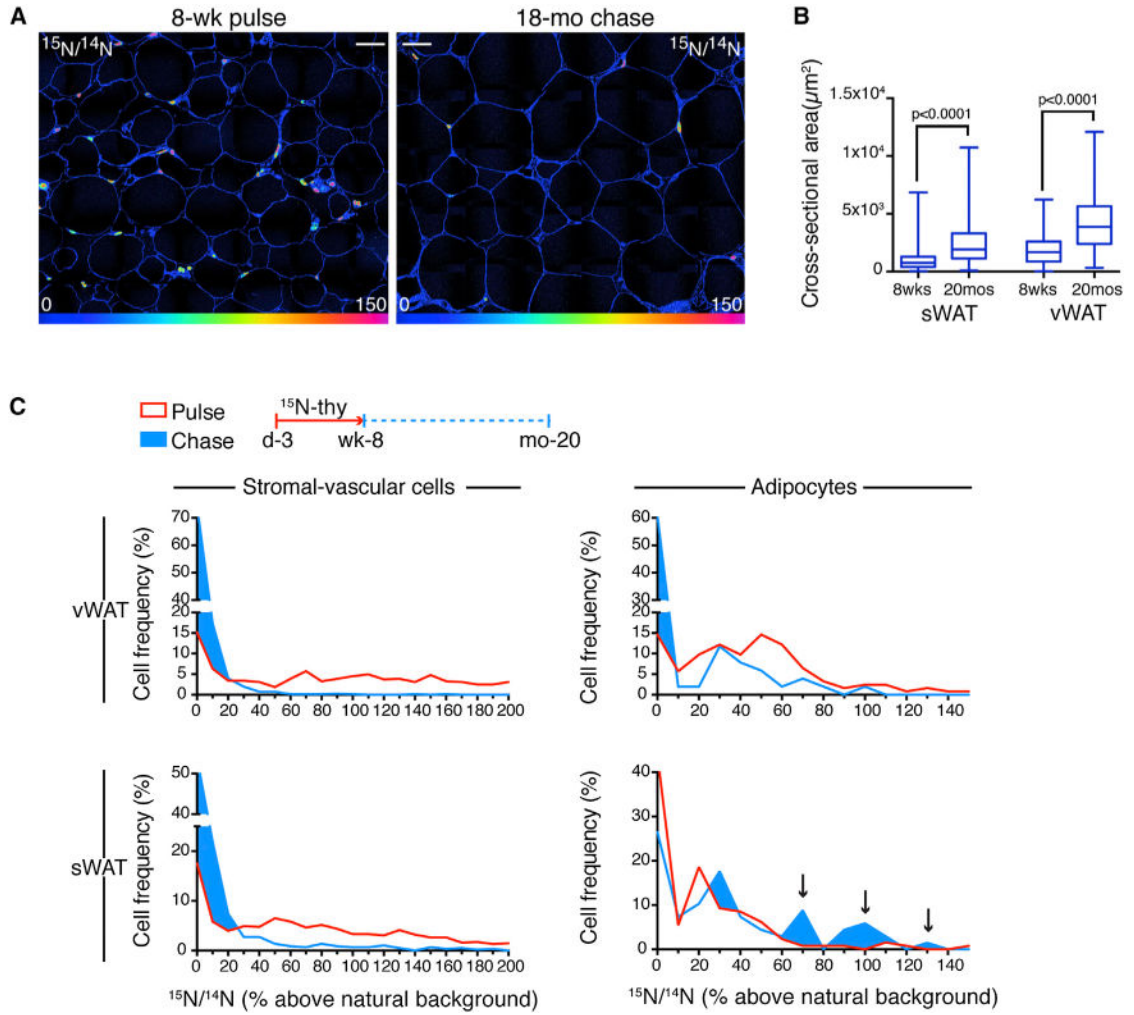


Figure 3. Limited Turnover of Subcutaneous Adipocytes with Aging

(A) ^{15}N -thymidine administered postnatal day 4 through week 8, followed by 18 month chase. WAT after pulse (left) and pulse-chase (right). ^{15}N -labeling is reduced with chase. Grossly larger adipocytes are seen in the old mice. HSI mosaic images constructed from 60 μm tiles. Scale bar represents 30 μm .

(B) Box plots of adipocyte size distributions as a function of age and depot (whiskers show max/min, $n = 519\text{--}955$ cells/depot).

(C) Frequency distributions after pulse (red) and pulse-chase (blue) as a function of nuclear labeling intensity (y axis). A significant downshift in stromal vascular cell labeling was seen in vWAT (V: top left) and sWAT (SC: bottom left) depots, consistent with turnover ($\chi^2 p < 0.0001$). Visceral adipocytes (top right) also showed label dilution ($\chi^2 p < 0.0001$), but to a lesser degree than SV cells (43% of adipocytes retaining label compared to 88% labeled after pulse). sWAT adipocytes (bottom right) paradoxically showed reverse dilution. The frequency of unlabeled adipocytes decreased (pulse = 44%; chase = 26%, $\chi^2 p < 0.01$), due to an increase in highly labeled adipocytes (arrows). Pooled analysis of $n = 3$ mice/group. See also Figures S3 and S5.

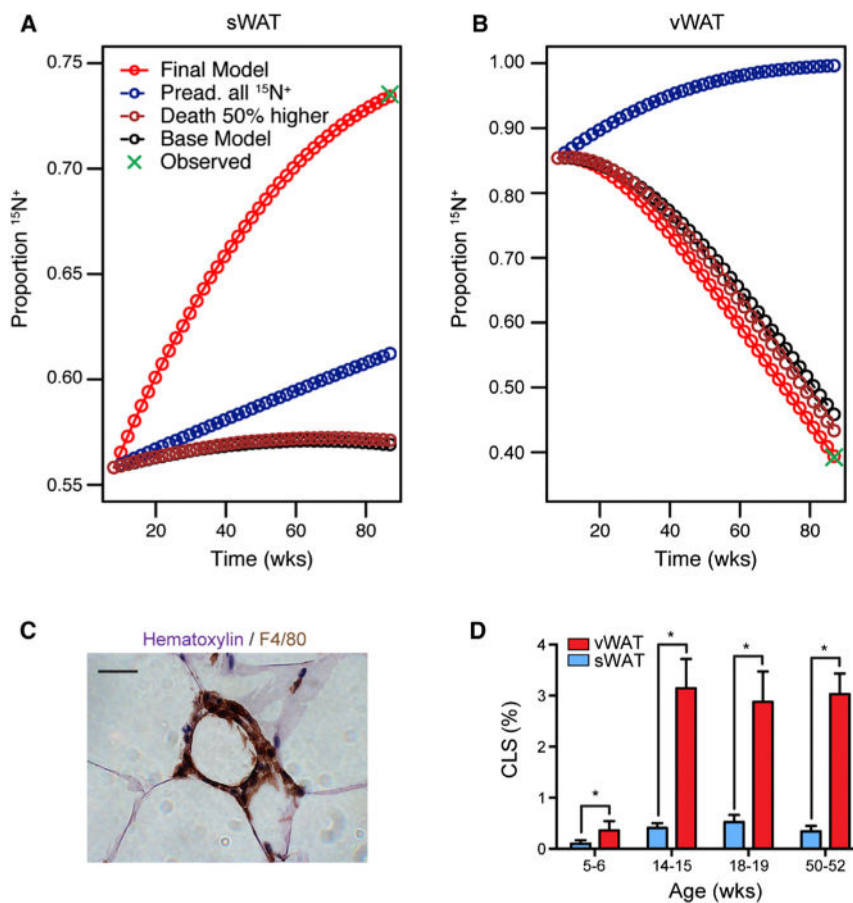


Figure 4. Modeling Adipocyte Turnover

(A) Simulated models of sWAT adipocyte turnover. Increasing the adipocyte death rate (Death 50% higher) did not substantially improve the fit of the model. Even an assumption of 100% progenitor ^{15}N -labeling at conclusion of pulse was insufficient to simulate the observed data. The data were best fit by the inclusion of progenitor differentiation without further division (Final Model).

(B) Modeling of vWAT adipocyte turnover.

(C) Representative “crown-like structure.” F4/80 staining macrophages surrounding a necrotic adipocyte. Scale bar represents 20 μm .

(D) Relative frequencies of “crown-like structures” in the sWAT and vWAT of C57BL/6 mice as a function of age (mean \pm SEM; $n = 3-7$).

See also Figure S6, Table S1, and Supplemental Experimental Procedures.

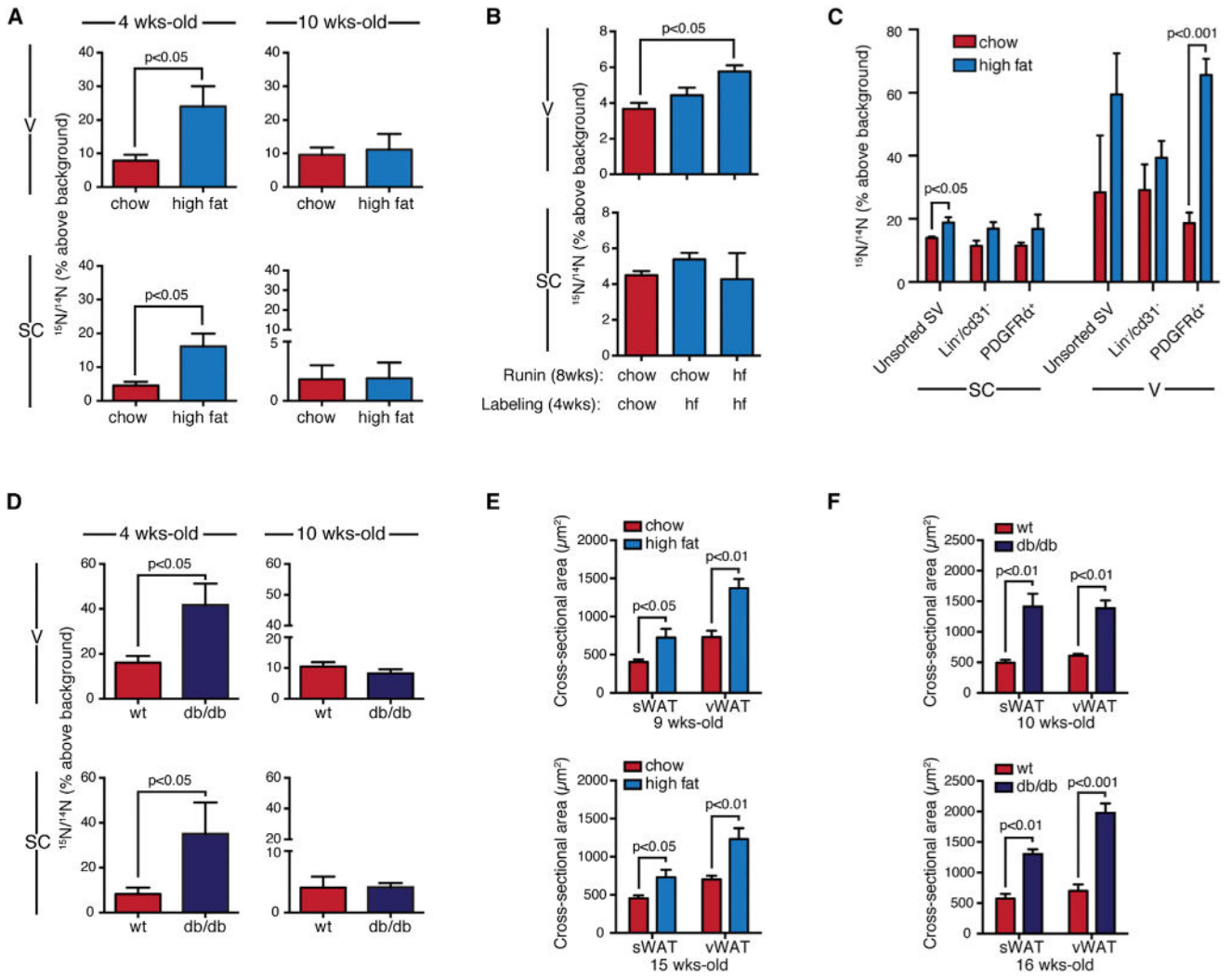


Figure 5. Obesity-Associated Adipose Tissue Plasticity Is Lost in the Adult

(A) Diet-induced obesity. Four-week-old mice showed increased ^{15}N -labeling of adipocytes with high-fat diet (mean \pm SEM; $n = 7-8$ mice per group; $p < 0.05$). No difference was seen in 10-week-old mice, studied in parallel. ^{15}N -thymidine pulse for 2 weeks, followed by 3 week chase.

(B) An 8 week high-fat run-in increased ^{15}N -labeling of visceral, but not subcutaneous, adipocytes (mean \pm SEM; $n = 3-7$ mice/group).

(C) Proliferative activity of progenitor-containing stromal vascular fractions. Mice administered chow or high-fat diet for 8 weeks prior to ^{15}N -thymidine for 1 week. Data expressed as mean \pm SEM; $n = 3-4$ /group.

(D) Increased ^{15}N -labeling of adipocytes was observed in 4-week-old *Lepr^{db}/Lepr^{db}* (*db/db*) mice compared to WT controls (mean \pm SEM; $n = 5-6$ mice per group, $p < 0.05$). Significant differences were not observed in adults (10 weeks). ^{15}N -thymidine pulse for 2 weeks, followed by 4 week chase.

(E) Mean adipocyte size (\pm SEM) after high-fat feeding at the conclusion of the labeling experiment described in (A).

(F) Mean adipocyte size (\pm SEM) in db/db mice versus WT mice at the conclusion of the labeling experiment described in (D).
WAT fractions were analyzed by IRMS. Each replicate is from a single mouse depot. See also Figure S3.

Author Manuscript

Author Manuscript

Author Manuscript

Author Manuscript

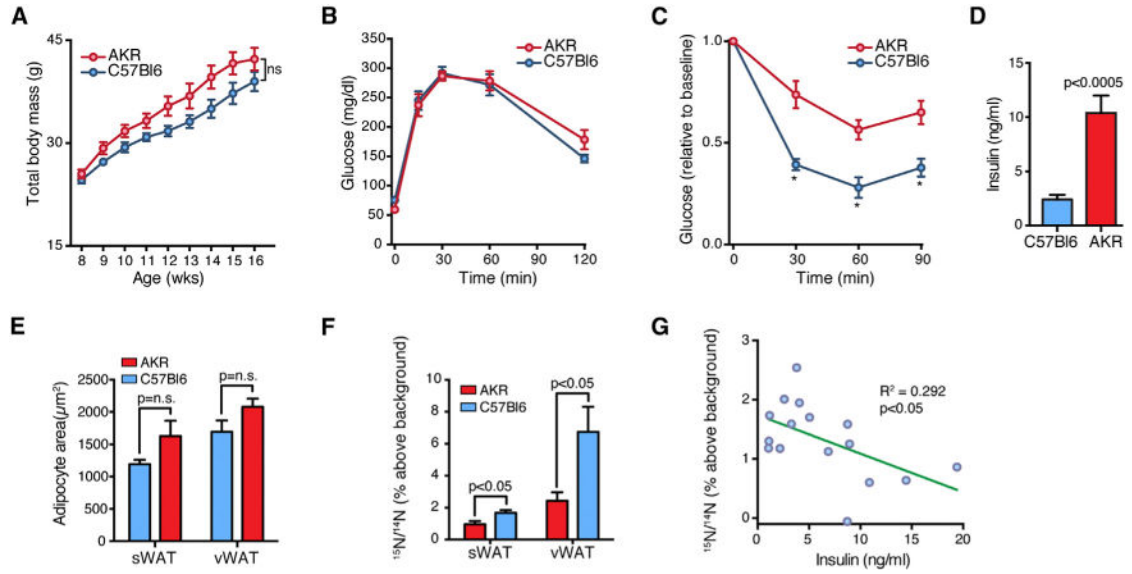


Figure 6. Impaired Adipocyte Turnover Is Associated with Insulin Resistance

(A) Weight gain during 8 weeks of high-fat feeding of C57BL/6 and AKR mice. Data expressed as mean ± SEM.

(B) Intraperitoneal (1.5 g/kg) glucose tolerance testing. Data expressed as mean ± SEM.

(C) Intraperitoneal (0.75 U/kg) insulin tolerance testing shows heightened insulin resistance in AKR mice relative to C57BL/6 mice. Data expressed as mean ± SEM, * $p < 0.05$.

(D) Mean serum insulin (±SEM) levels are higher in AKR mice, consistent with insulin resistance.

(E) Bar graph showing mean adipocyte cross-sectional area (±SEM) in C57BL/6 and AKR mice after 8.5 weeks high-fat feeding ($n = 8$ mice/strain).

(F) ^{15}N -labeling shows higher indices of adipogenesis in C57BL/6 mice compared to AKR mice. Data expressed as mean ± SEM.

(G) Negative correlation between sWAT ^{15}N -thymidine labeling of adipocytes and circulating insulin levels.

See also Figure S3.